UC Santa Barbara
UC Santa Barbara Previously Published Works

Title

Magnetic sulfide-modified nanoscale zerovalent iron (S-nZVI) for dissolved metal ion removal

Permalink

https://escholarship.org/uc/item/72p552w6

Authors

Su, Yiming
Adeleye, Adeyemi S
Keller, Arturo A
et al.

Publication Date

2015-05-01

DOI

10.1016/j.watres.2015.02.004

Peer reviewed
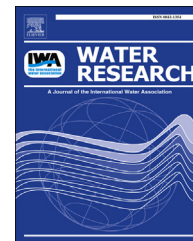
ELSEVIER

Magnetic sulfide-modified nanoscale zerovalent iron (S-nZVI) for dissolved metal ion removal

CrossMark

Yiming Su [a,b,c], Adeyemi S. Adeleye [b,c], Arturo A. Keller [b,c,*],
Yuxiong Huang [b], Chaomeng Dai [a,d], Xuefei Zhou [a], Yalei Zhang [a,e,**]

[a] State Key Laboratory of Pollution Control and Resources Reuse, Tongji University, Shanghai 200092, China
[b] Bren School of Environmental Science & Management, University of California, Santa Barbara, 3420, Bren Hall, CA 93106, USA
[c] University of California Center for Environmental Implications of Nanotechnology, Santa Barbara, CA, USA
[d] College of Civil Engineering, Tongji University, Shanghai 200092, China
[e] Key Laboratory of Yangtze Water Environment for Ministry of Education, Tongji University, Shanghai 200092, China

ARTICLE INFO

ABSTRACT

Sulfide-modified nanoscale zerovalent iron (S-nZVI) is attracting a lot of attention due to its ease of production and high reactivity with organic pollutants. However, its structure is still poorly understood and its potential application in heavy metal remediation has not been explored. Herein, the structure of S-nZVI and its cadmium (Cd) removal performance under different aqueous conditions were carefully investigated. Transmission electron microscopy (TEM) with an energy-dispersive X-ray spectroscopy (EDS) analysis suggested that sulfur was incorporated into the zerovalent iron core. Scanning electron microscopy (SEM) with EDS analysis demonstrated that sulfur was also homogeneously distributed within the nanoparticles. When the concentration of $Na_2S_2O_4$ was increased during synthesis, a flake-like structure (FeS_x) increased significantly. S-nZVI had an optimal Cd removal capacity of 85 mg/g, which was >100% higher than for pristine nZVI. Even at pH 5, over 95% removal efficiency was observed, indicating sulfide compounds played a crucial role in metal ion removal and particle chemical stability. Oxygen impaired the structure of S-nZVI but enhanced Cd removal capacity to about 120 mg/g. Particle aging had no negative effect on removal capacity of S-nZVI, and Cd-containing mixtures remained stable in a two months experiment. S-nZVI can efficiently sequester dissolved metal ions from different contaminated water matrices.

© 2015 Elsevier Ltd. All rights reserved.

* Corresponding author. Bren School of Environmental Science & Management, University of California, Santa Barbara, 3420 Bren Hall, CA 93106, USA. Tel.: +1 8058937548; fax: +1 8058937612.
** Corresponding author. State Key Laboratory of Pollution Control and Resources Reuse, Tongji University, Shanghai 200092, China. Tel.: +86 2165982503; fax: +86 2165988885.
E-mail addresses: keller@bren.ucsb.edu (A.A. Keller), zhangyalei@tongji.edu.cn (Y. Zhang).

1.   Introduction

Cadmium (Cd) is a potentially carcinogenic heavy metal, which can accumulate in humans, and damage organs such as lungs, kidneys, and liver (Comba et al., 2012). Cd pollution is a common problem around the world (Kaushik et al., 2003; Monteiro-Neto et al., 2003). According to a report released recently by Ministry of Environmental Protection of the People's Republic of China, Cd is the most serious heavy metal pollutant in China (China, 2014). Wastewater from electroplating and some metallurgical factories can be an important source of Cd pollution, at typical concentrations of 40 mg/L (Zhang et al., 1993). nZVI has proven an efficient material for Cd immobilization (Zhang et al., 2014; Su et al., 2014a). Although compared to coagulation, precipitation, ion exchange and membrane separation, nZVI has its own advantages such as in-situ application, low solid waste product (easy to be separated and disposed) (Li 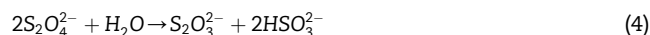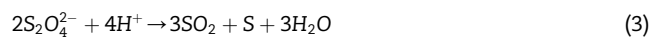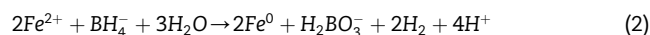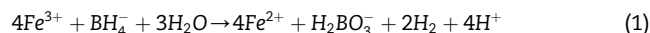et al., 2014), and stable removal performance regardless of the change of volume of water treated (Zhang et al., 2013), considering the cost (~$100/kg) (Crane and Scott, 2012) vis-à-vis its removal capacity (~40 mg/g) (Su et al., 2014a), nZVI-based could be more cost-effective if metal removal capacity could be improved. Furthermore, the presence of nitrate or oxygen decreases nZVI's removal efficiency due to oxidation (Adeleye et al., 2013; Su et al., 2014b). As a result, the Fe–Cd complex formed is often unstable (Zhang et al., 2014), which could be the main reason why nZVI is not suitable for in-situ remediation for heavy metal pollution. Hence, it is necessary to improve the removal capacity while enhancing the thermodynamic stability of immobilized Cd.

Given that FeS can effectively remove Cd^{2+}, Hg^{2+}, AsO_3^{3-}, and UO_2^{2+} from water (through adsorption, co-precipitation, and/or reduction) (Gallegos et al., 2013; Bi and Hayes, 2013; Morgan et al., 2012; Liu et al., 2008), sulfidized nZVI (S-nZVI) is likely to have high removal capacity for heavy metals while maintain its magnetism. Furthermore, metal sulfides are very stable as indicated by their low solubility product constant (Table S1), which means immobilized metals are not likely to be released into water again. Recent studies indicate that S-nZVI has a higher surface area and reactivity, but lower isoelectric point (IEP) than nZVI (Kim et al., 2011, 2013a). These characteristics, together with a simple synthesis process (titrating a mixture of sodium borohydride and dithionite into ferric solution) (Kim et al., 2011, 2013a), make S-nZVI an ideal material for heavy metal removal from water bodies. Sulfidation may decrease the toxicity of nZVI as seen in other nanoparticles (e.g. silver, (Reinsch et al., 2012)). Also, Kim et al. find nZVI coated with CdS exhibits limited toxicity to *Escherichia coli*. (Kim et al., 2013b). In addition, since pristine nZVI will undergo sulfidation in sulfate-reducing conditions (Rickard, 1995; Jeong et al., 2008), investigating the Cd removal mechanism of S-nZVI can shed some light on the transformation of nZVI when it is used for Cd removal under sulfate-reducing conditions.

However, until now, the structure of S-nZVI is still not well-understood. S-nZVI is generally conceived as an Fe^0 core with FeS shell (Kim et al., 2011), but when the mixture of sodium borohydride and dithionite is added into ferric solution, reduction (Eqs. (1) and (2)) (Li and Zhang, 2006), self-decomposition of dithionite (Eqs. (3)–(5)) (Cermak and Smutek, 1975), and precipitation (Eq. (6)) (Mejia Likosova et al., 2013) can occur simultaneously. This means that a mixed (rather than pure Fe^0) core is likely to form. But to the best of our knowledge, this phenomenon has not been investigated. Aside from the core, the S-nZVI shell may be composed of iron sulfide and iron oxide, making it different from nZVI (which typically only has an iron oxide shell). In addition, adding different amounts of dithionite could lead to different degrees of sulfidation of nZVI, which may affect the physicochemical characteristics (e.g. magnetic force) and pollutant removal capacity of the particles formed.

For Cd removal, adsorption can occur via formation of Cd^{2+}-substituted FeS by surface ion exchange (Eq. (7)), and complexation of Cd^{2+} with reactive sites ($\equiv FeSH^+$) (Eq. (8)), similar to Hg^{2+} immobilization (Jeong et al., 2007). Co-precipitation (formation of $Fe_{(1-x)}Cd_xS$ complexes by $FeSH^+$ and Cd^{2+} in solution) may also occur (Eq. (9)). These two reactions (adsorption and co-precipitation) could be affected by many factors such as initial dithionite concentration (thus S content of particle), pH, dissolved oxygen, and aging. A previous study suggests that different dithionite concentrations affect the reactivity of synthesized particles with TCE (Jeong et al., 2008). pH may affect the solubility of S-nZVI, as observed for nZVI (Zhang et al., 2013). Dissolved oxygen and aging are likely to decrease the amount of nZVI (Adeleye et al., 2013) and influence FeS transformation (Bi et al., 2013). However, the effect of all these factors on the performance of S-nZVI is not well-understood.

$$4Fe^{3+} + BH_4^- + 3H_2O \rightarrow 4Fe^{2+} + H_2BO_3^- + 2H_2 + 4H^+ \tag{1}$$

$$2Fe^{2+} + BH_4^- + 3H_2O \rightarrow 2Fe^0 + H_2BO_3^- + 2H_2 + 4H^+ \tag{2}$$

$$2S_2O_4^{2-} + 4H^+ \rightarrow 3SO_2 + S + 3H_2O \tag{3}$$

$$2S_2O_4^{2-} + H_2O \rightarrow S_2O_3^{2-} + 2HSO_3^{2-} \tag{4}$$

$$S_2O_4^{2-} + S_2O_3^{2-} + 2H_2O + H^+ \rightarrow 3HSO_3^{2-} + H_2S \tag{5}$$

$$Fe^{2+}/Fe^{3+} + S^{2-} \rightarrow FeS/Fe_2S_3 \tag{6}$$

$$\equiv FeS + xCd^{2+} \rightarrow \equiv Fe_{(1-x)}Cd_xS + xFe^{2+} \tag{7}$$

$$\equiv FeSH^+ + Cd^{2+} \rightarrow \equiv FeS - Cd^{2+} + H^+ \tag{8}$$

$$FeSH^+ + xCd^{2+} \rightarrow Fe_{(1-x)}Cd_xS + xFe^{2+} + H^+ \tag{9}$$
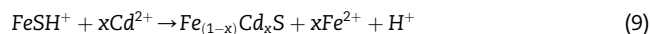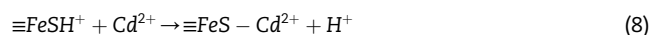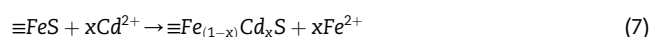
The objectives of this research were to evaluate the influence of addition of different dithionite amounts during the synthesis of S-nZVI on the structure and performance of S-nZVI, as well as to investigate how dissolved oxygen, pH, and aging may influence Cd removal by S-nZVI. This study also assessed the practical utilization of S-nZVI for heavy metal pollution in-situ remediation in natural water systems.

2. Material and methods

2.1. Chemical reagents

Analytical grade cadmium chloride ($CdCl_2$), zinc chloride ($ZnCl_2$), nickel chloride ($NiCl_2$), cobalt chloride ($CoCl_2$), sodium borohydride ($NaBH_4$, 98%), dithionite ($Na_2S_2O_4$), ferric chloride anhydrous ($FeCl_3$), sodium hydroxide (NaOH) and hydrochloric acid (HCl) were purchased from Fisher Scientific (Pittsburgh, PA). All chemicals were used without further purification. Nanopure water (18.2 MΩ cm, Barnstead) was used for all reagent and particle suspension preparation.

2.2. nZVI and S-nZVI synthesis methods

nZVI and S-nZVI were synthesized using the method described by Kim et al. (2011). Briefly, 250 ml 7.6 g sodium borohydride with different amounts of dithionite (0, 0.125, 0.25, 0.5, 0.75, and 1 g) were separately introduced into 250 ml $FeCl_3$ solution (4.9 g) via titration (titration rate ~1 L/h), to achieve S/Fe molar ratios of 0 (or nZVI), 0.035, 0.07, 0.14, 0.21, and 0.28. Preliminary results showed that particles were no longer magnetic above an S/Fe ratio of 0.28, so we only considered S/Fe ratios ≤0.28. After reduction, nanoparticles were collected and washed with nanopure water three times. A neodymium–iron–boron magnet was used to separate solids and liquids. Fresh nZVI and S-nZVI were stored in 30% ethanol at 4 °C to reduce oxidization.

2.3. Cd removal performance of S-nZVI particles with different S/Fe ratios

To simulate oxygen limited conditions, 0.71 ml S-nZVI stock suspension (S-nZVI concentration, ~35 g/L) were added to 50 ml solutions with different initial Cd concentration (10, 20, 40, or 80 mg/L) in 50 ml polypropylene tubes tightly capped. The tubes had minimal headspace, to provide a low oxygen condition with low resupply of oxygen. The tubes were shaken (90 rpm) on an end-over-end shaker (Dayton-6Z412A Parallel Shaft roller mixer) at room temperature (22 °C). After 2 h (preliminary tests indicated that Cd adsorption after 2 h was very limited), the magnet was used to separate the S-nZVI particles from the liquid and 1 ml supernatant was collected for metal analyses. After acidifying the aliquot with 10% ultrahigh-purity HNO_3 (total sample volume = 10 ml), Cd, Fe and S concentrations were measured via inductively coupled plasma atomic emission spectroscopy (ICP-AES, iCAP 6300, Thermo Scientific).

2.4. Effect of oxygen on Cd removal by nZVI and S-nZVI

S-nZVI with an S/Fe ratio of 0.28 was used in these experiments due to its high Cd removal capacity and magnetism (for solid–liquid separation). Suspensions (250 ml) with S-nZVI (500 mg/L) mixed in with dissolved Cd (20, 30, 40, 50, 60, 70, 80, 90, or 100 mg/L) in a 500 ml flask were agitated by an electric stirrer (250 rpm) at room temperature, continuously supplying dissolved oxygen to the reaction system (a high oxic condition). During stirring, 5 ml samples (to ensure the samples

represent the whole mixture) were removed at different times (15, 30, 45, 60, 90, 120, and 180 min) and 1 ml aliquots were collected from a 1.5 ml tube after centrifugation (Thermo Scientific, Legend Micro 21R) and analyzed for Cd, total S, and total Fe via ICP-AES. At the end of the tests, to analyze the main composition (Fe, Cd, S) of residual oxidized particles, five 10 ml mixtures (liquid and particles) were collected (in 15 ml polypropylene tubes) and 1 ml liquid was extracted at the 6 ml mark at different times (15, 30, 60, 90, 120 min) for ICP-AES analysis after acidifying.

2.5. pH effect on Cd removal

Certain amount of S-nZVI stock suspension were added to six 50 ml Cd solutions (40 mg/L) at pH 4, 5, 6, 7, 8, and 9; using 0.05 and 0.1 M NaOH and HCl to adjust pH. After 2 h reaction, 1 ml supernatant was collected for Cd, Fe, and S analyses via ICP-AES.

2.6. Aging effect on Cd removal

A certain amount of three-week old (aged in nanopure water) nZVI or S-nZVI suspension were introduced into 10, 20, 40, or 80 mg/L Cd solutions (50 ml final volume, in polypropylene tubes) to achieve a concentration of 500 mg/L. Tubes were shaken using the roller mixer at 90 rpm. After 2 h reaction, aliquots were collected from supernatant and analyzed for Cd, Fe, and S.

2.7. Removal of different heavy metals by S-nZVI

A certain volume of S-nZVI stock solution was added into four separate heavy metal solutions (Ni, Zn, Co, and Cd, each at 50 mg/L), to achieve an S-nZVI concentration of 500 mg/L. The total volume of the mixture was about 50 ml, leaving minimal headspace in the 50 ml polypropylene tubes. After 2 h shaking, 1 ml of supernatant was collected and analyzed via ICP for total Fe and heavy metal.

2.8. Cd removal performance in different water bodies

Five different surface waters were used in this experiment, namely seawater (Pacific Ocean collected at Santa Barbara, CA) (Adeleye and Keller, 2014), river water (Upper Middle Creek in Malibu, CA), groundwater (collected from a monitoring well in Santa Barbara), wastewater (secondary effluent of EI Estero Wastewater Treatment Plant, Santa Barbara) (Adeleye and Keller, 2014), and nanopure water. The composition of these waters is in the supporting material (Table S2). 50 mL mixtures containing 500 mg/L nZVI or S-nZVI and 50 mg/L Cd^{2+} ions were shaken on the roller mixer for 2 h. 1 ml aliquots were collected and analyzed for Cd and Fe.

2.9. Analyses

Transmission electron microscopy (TEM, FEI Titan 300 kV FEG) attached with an Oxford energy-dispersive X-ray spectroscopy (EDS) system and an FEI Co. XL30 FEG wet-mode environmental scanning electron microscopy (ESEM) (Philips Electron Optics, Eindoven, The Netherlands) with EDS were

employed to investigate the structure of the nanoparticles. A Zetasizer Nano-ZS90 (Malvern, UK) was used to determine the zeta (ζ) potential of particles. X-ray diffraction (XRD, Bruker D8 Advance) was utilized to analyze the crystal structure of the material. X-ray photoelectron spectrometry (XPS, Kratos Ultra) was used to analyze the surface composition of the material. The Brunauer–Emmett–Teller (BET) specific surface area was measured through N_2 adsorption method using a TriStar 3000 system (Micromeritics Corp., USA). UV–Vis spectrometer (Biospec-1601, Shimadzu, Japan) was used to obtain spectrum of the nanoparticle mixture from 190 to 1100 nm. ICP-AES was used to measure the concentration of Cd, S, Ni, Co, Zn, and total Fe.
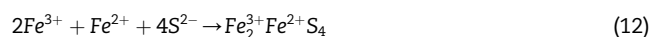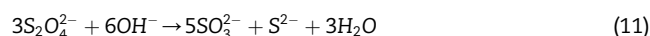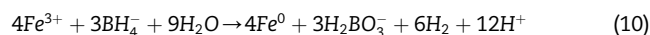
3. Results and discussion

3.1. Characteristics of FeS-nZVI

According to previous studies, pristine nZVI particles have an almost spherical core–shell structure and exhibit chain-like particle aggregation (Li and Zhang, 2006; Zhang et al., 2013). TEM images show that S-nZVI has a different morphology compared to nZVI. S-nZVI has a flake-like shell, and unlike nZVI, the core does not have an obvious compact shell (Fig. 1a). Furthermore, the core of S-nZVI particles appears to be composed of very small particles, with several pore canals (Fig. 1b). Fig. S1 and Fig. S2 show that S-nZVI are almost spherical (diameter ~200 nm) though flaky. The level of flaking increases with increasing S/Fe ratio. A detailed investigation by SEM with EDS shows that Fe and S are uniformly distributed within S-nZVI regardless of the different amounts of flake-like structures (Fig. S3). EDS analysis shows that the S/Fe ratio in the core area is 18/81 and 10/85 in the flaky shell area (Fig. S4 and S5). This indicates that there is a significant amount of S in the core.

The morphology and composition of S-nZVI is probably due to the synthesis process, which can be divided into a number of phases. During the initial synthesis phase, the pH of the $FeCl_3$ solution increases from <1 to ~4 due to the

addition of the mixture of $NaBH_4$ and $Na_2S_2O_4$ (solution pH ~10). Fe^{3+} can only be reduced to Fe^{2+} (Eq. (1)), but the decomposition of $Na_2S_2O_4$ is accelerated, which results in the production of S^0 (Eq. (3)) (Ulrich, 2004). In the following phase, pH increases from ~4 to ~8, generating a large amount of Fe^0 (Eqs. (2) and (10)) (Bi et al., 2013), and the high S content within the core from EDS analysis indicates that the former S^0 particles are incorporated into Fe^0 nanoparticles. Later, as the amount of $Na_2S_2O_4$ introduced into solution increases, a large amount of H_2S will be generated (Eq. (5)) (Rickard, 1995), followed by the formation of ferrous sulfide (FeS), ferric sulfide (Fe_2S_3) (Eq. (6)).

In the next stage, with continuous introduction of $NaBH_4$, the pH increases from ~8 to ~10, leading to a strong reaction between $Na_2S_2O_4$ and OH^- (Eq. (11)) (Ulrich, 2004) and further facilitating the formation of outside flake-like structure. Through analyzing S2p region of XPS, the surface compositions of S-nZVI are much clear. In Fig. 2, the doublets due to the spin–orbit splitting of S2$p_{1/2}$ and S2$p_{3/2}$ (Herbert et al., 1998) for greigite ($Fe_2^{3+}Fe^{2+}$,S_4, possibly formed by Eq. (12)), polysulfide (S_n^{2-}, often found in reducing conditions with the presence of sulfur compounds), SO_3^{2-}, and SO_4^{2-} are associated with the binding energy at 160.8 eV (162.0 eV), 163.8 eV (165.0 eV), 166.6 eV (167.8 eV), and 168.6 eV (170.0 eV), respectively, in accordance with the study by Neal et al. (2001); In addition, due to the relatively low concentration of $Na_2S_2O_4$, an iron oxide shell can still be identified surrounding the core. Hence, S-nZVI acquires a specific structure: an Fe^0 and S^0 mixed core surrounded by iron oxide and flake-like shell.

$$4Fe^{3+} + 3BH_4^- + 9H_2O \rightarrow 4Fe^0 + 3H_2BO_3^- + 6H_2 + 12H^+ \qquad (10)$$

$$3S_2O_4^{2-} + 6OH^- \rightarrow 5SO_3^{2-} + S^{2-} + 3H_2O \qquad (11)$$

$$2Fe^{3+} + Fe^{2+} + 4S^{2-} \rightarrow Fe_2^{3+}Fe^{2+}S_4 \qquad (12)$$

The IEP of nZVI and S-nZVI is around pH 7.5 and ~5 respectively (Figure S6). The IEP of S-nZVI does not change much with the variation of S/Fe ratio, indicating that FeS (IEP = pH 0.8–3.5) (Dekkers and Schoonen, 1994) on the surface influences the surface charge (even at low S/Fe ratio). This
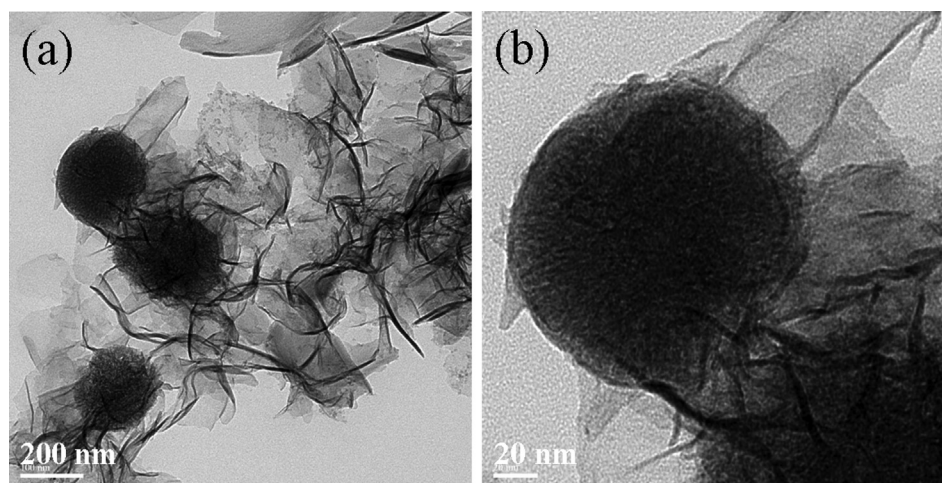

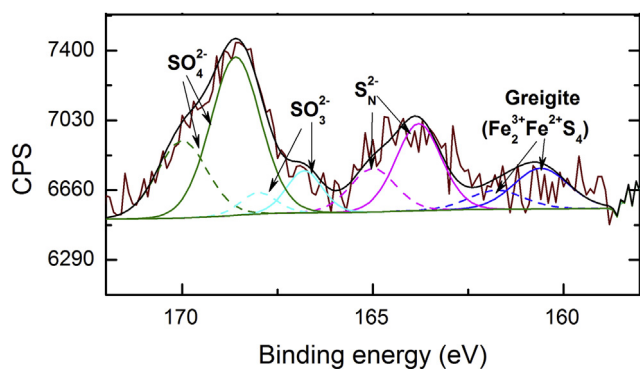Fig. 1 – TEM images of S-nZVI particles with S/Fe ratio of 0.28.

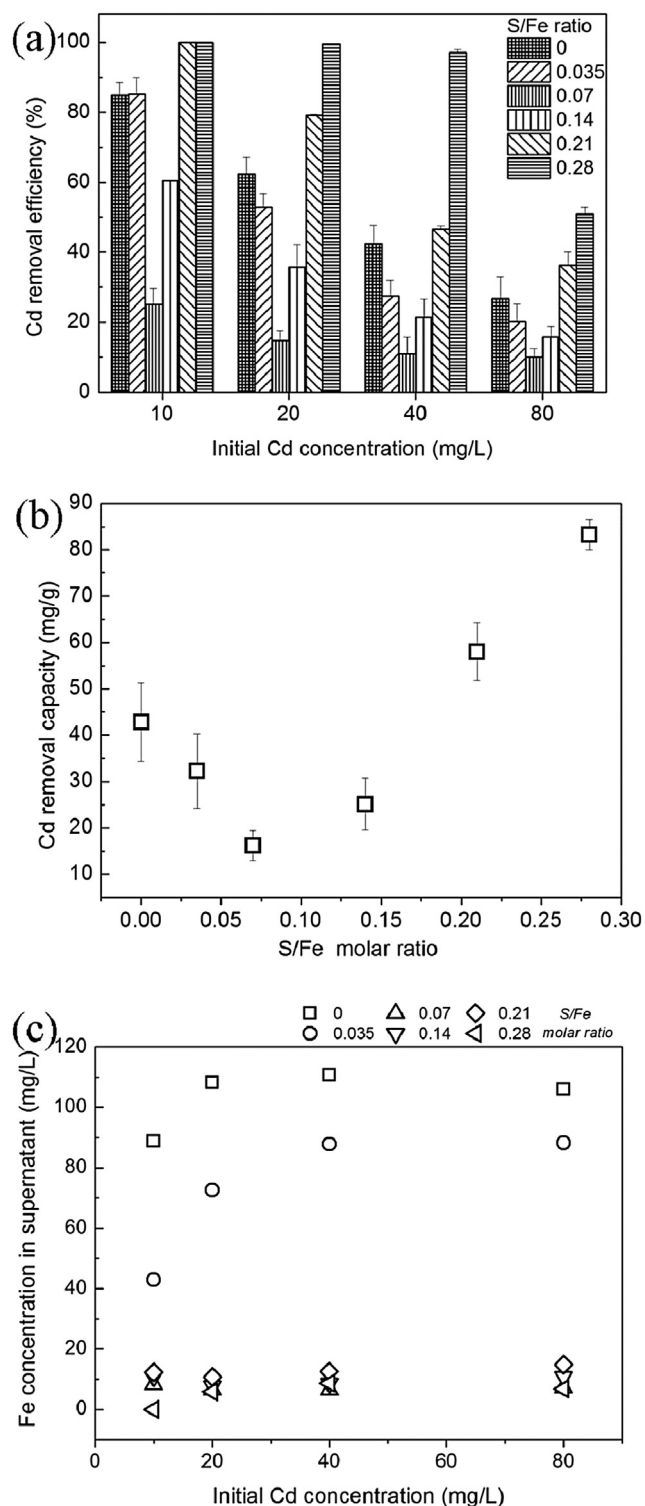**Fig. 2 – S2p XPS spectrum of fresh S-nZVI.**

Fig. 3 – (a) Cd removal efficiency of S-nZVI with different S/Fe ratio; (b) Cd removal capacity of S-nZVI with different S/Fe ratio; (c) Fe concentration in final supernatant after Cd adsorption with different types of S-nZVI (nanoparticle concentration = 500 mg/L).

result is in line with Kim et al. (2013a). A low IEP implies that S-nZVI will be negatively charged in most natural water systems, which may contribute to Cd^{2+} removal via electrostatic interaction.

Figure S7 shows the XRD patterns of nZVI and S-nZVI, which indicate the presence of Fe^0 ($2\theta = 44.6°$) in S-nZVI, just like nZVI (Adeleye et al., 2013; Zhang et al., 2013). While a small peak of iron oxide ($2\theta = 35.4°$) is detected in S-nZVI, no clear S^0 or any iron sulfide peak is observed.

3.2. Effect of different S/Fe ratios on Cd removal performance

The S/Fe ratio strongly influences Cd removal performance of S-nZVI. Fig. 3a shows that at the same initial Cd concentration, as the S/Fe ratio increases Cd removal efficiency decreases initially, and then increases. While Cd removal capacity of nZVI is about 42.5 mg/g, S-nZVI has a minimum Cd removal capacity of 15 mg/g (at S/Fe ratio = 0.07), and a maximum capacity of 85 mg/g (at S/Fe ratio = 0.28) (Fig. 3b). The difference in removal capacity of different ratios of S/Fe in S-nZVI can be attributed to the different extent of sulfidation. As seen in Fig. 3c, a high concentration of Fe in the supernatant suggests that S-nZVI with an S/Fe ratio of 0.035 has similar characteristics to nZVI, which may be responsible for the similar removal capacity. The difference among Fe concentrations in the supernatant indicates the different extent of sulfidation, which may impart particles with different surface functional groups.

As we reported previously, the Fe concentration in solution could be an indicator of co-precipitation and adsorption for metal removal by nZVI (Zhang et al., 2013). It is likely that the relatively low S content of S-nZVI inhibits these two removal pathways of nZVI, as indicated by the low concentration of Fe ions in the supernatant. On the other hand, due to the low S content, the total amount of surface sulfhydryl group is limited. Thus, the decrease of Cd removal efficiency is observed when S/Fe ratio increases from 0 to 0.07. However, as S content increases (S/Fe ratio increases from 0.14 to 0.28) continuously, the surface sulfhydryl group increases as well, leading to an improvement in removal capacity.

In addition to the increased Cd removal, the sharp decline of dissolved Fe(II) ions in the supernatant after adsorption in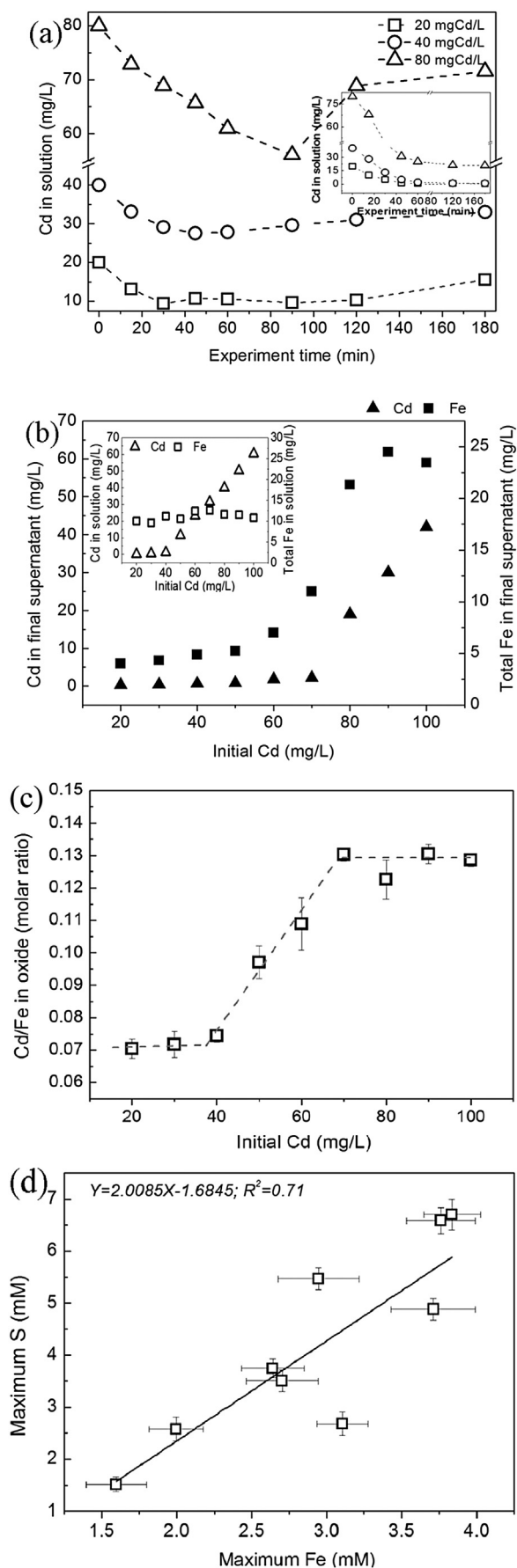dicates that S-nZVI will pose lower toxicity risks compared to nZVI, whose toxicity was partly due to Fe(II) ions in solution (Keller et al., 2012; Chen et al., 2013). In a recent study (Kim et al., 2013b), S-nZVI after Cd adsorption showed limited

(a)

(b)

(c)

(d)

$Y=2.0085X-1.6845; R^2=0.71$

toxicity to *E. coli*, unlike nZVI (Kim et al., 2010). Thus, S-nZVI has higher Cd removal capacity, and perhaps, better biocompatibility than nZVI.

3.3.   Enhanced Cd removal performance of S-nZVI under aerobic condition

As shown in Fig. 4a, under highly oxic conditions there is a slight increase in Cd concentration in the nZVI reaction system, but this is not observed in the S-nZVI reaction system (S/Fe = 0.28). In addition, Cd removal by S-nZVI is greater for high oxygen than in limited oxygen (Fig. 4a). For instance, at an initial Cd concentration of 80 mg/L, the final Cd concentration detected is 20 mg/L in oxic conditions and 40 mg/L in nearly anoxic conditions. As such, although oxygen has a negative influence on Cd removal by nZVI (Zhang et al., 2014), it has a positive effect on Cd removal by S-nZVI.

Fig. 4b indicates that in the presence of oxygen, Cd removal efficiency is ~100% when the initial Cd concentration is below 70 mg/L. However, in a nearly anoxic system, a considerable amount of Cd ions is detected when the initial Cd concentration exceeds 40 mg/L. Cd removal capacity of S-nZVI in the nearly anoxic system is 85 mg/g, and 120 mg/g when oxygen is present.

The other important difference between the two conditions is the trend of total Fe concentration in the supernatant. Total Fe concentration in systems with limited oxygen is constant at ~10 mg/L at all initial Cd concentrations tested. However, when oxygen is present Fe concentration is either ~5 mg/L (at initial Cd concentration below 70 mg/L) or ~20 mg/L (at initial Cd concentration above 70 mg/L). A sigmoidal relationship is observed between ratios of Cd/Fe in oxidized particles and initial Cd concentrations (Fig. 4c). At low levels of Cd ($\leq$40 mg/L), the Cd/Fe ratio in oxide is stable at ~0.07. The Cd/Fe ratio then increases rapidly to 0.13 for initial Cd between 40 and 70 mg/L, after which it again stabilizes.

When the initial Cd concentration is $\leq$40 mg/L, complete removal can be achieved by S-nZVI with or without oxygen. As the initial Cd concentration increases, more Cd^{2+} ions are incorporated in the Fe and S matrix, leading to an increase of the Fe/Cd ratio. Meanwhile, a considerable amount of sulfur is detected in the final oxide, and it correlates with iron content in the oxide. As shown in Fig. 4d, S content is twice as much as Fe content, as indicated by the slope of the line. High content of S favors the metal removal.

The increase of Cd removal capacity could be explained by XPS analysis (Fig. 5). In oxygen limited conditions (Fig. 5a), the S2*p* region can be decomposed into peaks at 161.4 eV (162.6 eV), 162.0 eV (163.2 eV), 168.6 eV (169.8 eV) (data in parenthesis means the position of satellite peak of each one)

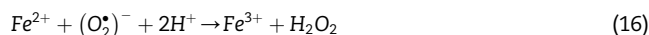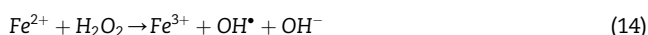**Fig. 4 − (a) Cd removal performance of nZVI and S-nZVI (inserted image) under oxic conditions; (b) Final Cd and Fe concentration in supernatant of nearly anoxic (inserted image) or oxic systems; (c) Fe/Cd molar ratio in final particles at different initial Cd concentrations under oxic conditions; (d) relationship between maximum Fe and S content in oxidized particles. (nanoparticle concentration = 500 mg/L).**
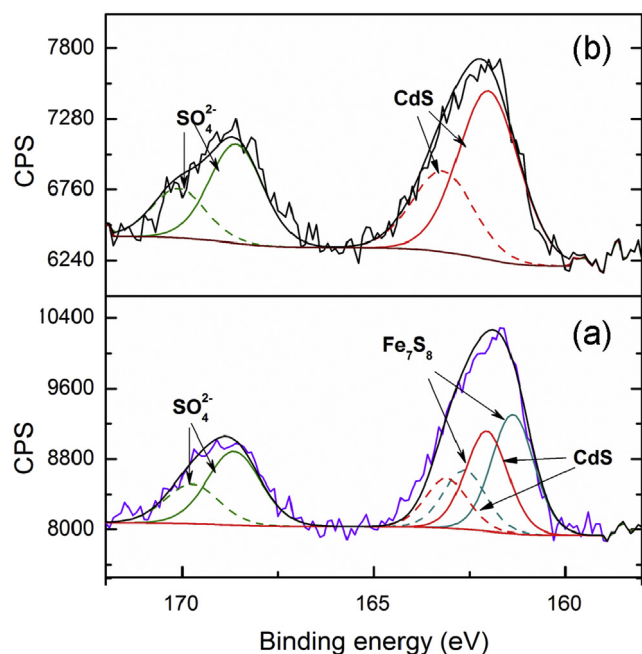
Fig. 5 – S2p XPS spectra of S-nZVI after Cd adsorption in oxygen limited conditions (a) and in oxic conditions (b) (initial Cd = 60 mg/L; nanoparticle concentration = 500 mg/L).

(Neal et al., 2001; Colvin et al., 1992), which represent S in Fe_7S_8, CdS, and SO_4^{2-}, respectively; in oxic conditions (Fig. 5b), the S2p spectrum indicates the existence of CdS and SO_4^{2-}. The appearance of CdS is further confirmed by Cd3d XPS spectrum (Fig. S8), in which the principal peaks locate at 405.4 eV and 412.2 eV (Hota et al., 2007). The difference of surface compositions between two different conditions explains the reason why Cd removal capacity increases under oxic conditions. Under oxic conditions, dissolved oxygen contributes to the break of interior Fe–S bonds in Fe_7S_8, converting them to sulfydryl groups for Cd^{2+} adsorption, consequently leading to the increase in Cd removal capacity.

Under oxic conditions, Fe^0, H^+, and O_2 will stimulate the formation of hydroxyl radicals (Eqs. (13) and (14)) (Yan et al., 2013), indicated by the peaks for hydroxyl radical (~250 nm) in the UV–Vis spectrum of S-nZVI with Cd under oxic conditions (Jayson et al., 1972) (Fig. S9). The hydroxyl radicals may further favor the break of Fe–S bonds in Fe_7S_8, as observed by a peak of $FeSH^+$ at around 320 nm (Tewari and Campbell, 1979). The derived $FeSH^+$ can react with Cd^{2+} in solution (Eq. (9)) to form $Fe_{(1-x)}Cd_xS$, which precipitates out of water. In addition, with O_2 present, Fe_7S_8 can also generate hydroxyl radicals (Eq. (15) and (16)) as reported by Li et al. (2012). Meanwhile, the S–S dumbbell bond in Fe_7S_8 is broken and a monosulfide component is formed (Murphy and Strongin, 2009). Due to the strong affinity between Cd^{2+} and monosulfide, Cd^{2+} ions in solution are adsorbed onto the surface rapidly (Eqs. (7) and (8)).

$$Fe^0 + 2H^+ + O_2 \rightarrow Fe^{2+} + H_2O_2 \tag{13}$$

$$Fe^{2+} + H_2O_2 \rightarrow Fe^{3+} + OH^\bullet + OH^- \tag{14}$$

$$Fe^{2+} + O_2 \rightarrow Fe^{3+} + \left(O_2^\bullet\right)^- \tag{15}$$

$$Fe^{2+} + \left(O_2^\bullet\right)^- + 2H^+ \rightarrow Fe^{3+} + H_2O_2 \tag{16}$$

The influence of oxygen on Cd removal by S-nZVI was also analyzed via SEM and TEM. In limited oxygen, the structure of S-nZVI did not change significantly: the flake-like structure was not destroyed (Fig. S10) and the majority of the core remained (Fig. S11). However, with oxygen present, the structure of S-nZVI changed remarkably. Flocculent deposits with a needle-like framework (average length of 220 nm) were observed (Fig. 6a and b).

3.4. pH effect on Cd removal performance

As in the case of pristine nZVI (Zhang et al., 2013), pH influences both dissolution and Cd removal of S-nZVI (S/Fe ratio = 0.28) (Fig. 7). However, while pH 5 causes complete nZVI dissolution, pH 4 only leads to partial S-nZVI dissolution. The sharp increase in Cd removal efficiency and
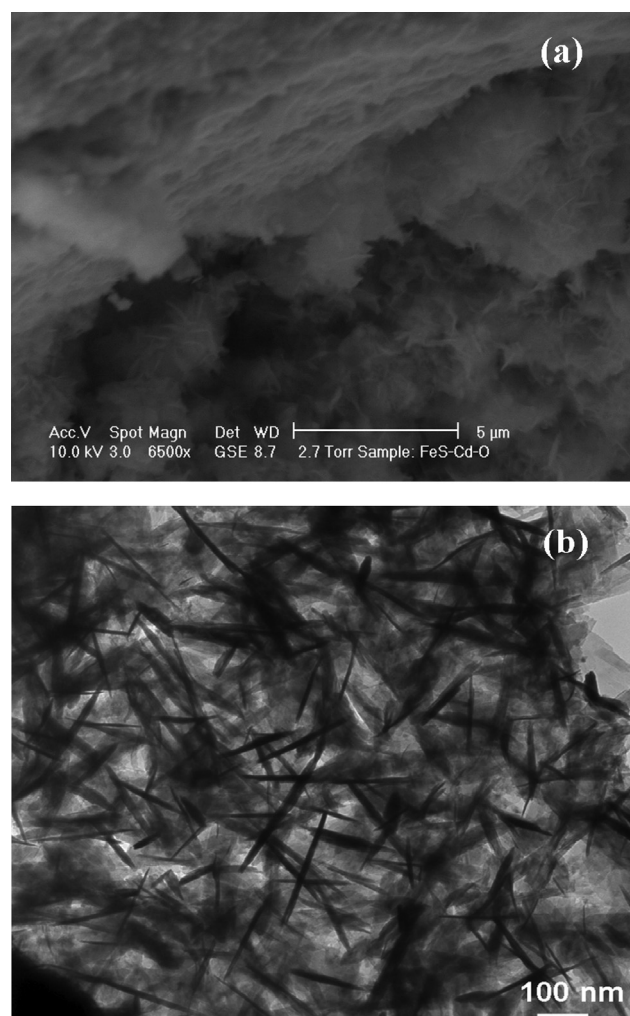
Fig. 6 – SEM and TEM images of S-nZVI particles (S/Fe, 0.28) derived from Cd adsorption system with oxygen (initial Cd = 60 mg/L; nanoparticle concentration = 500 mg/L).
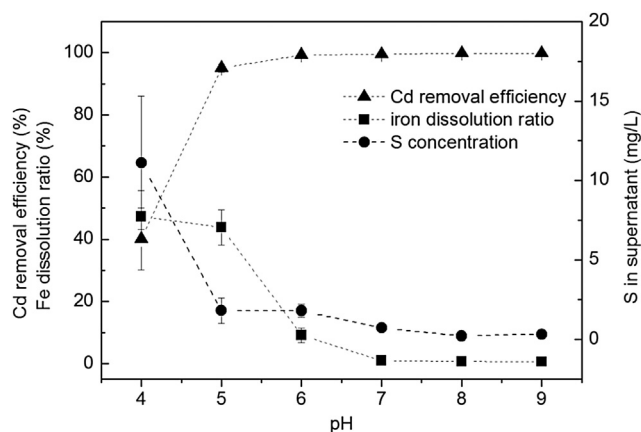
Fig. 7 – pH effect on Cd removal performance by S-nZVI (initial Cd concentration = 40 mg/L; nanoparticle concentration = 500 mg/L; error bar represents standard deviation).

decrease in Fe and S concentration as pH increases from 4 to 5 underscores the benefit of using S-nZVI for Cd removal compared to n-ZVI. About 40% Cd removal efficiency is obtained even at pH 4 probably due to the relative stability of S-nZVI. From pH 5 to 7, high Cd removal efficiency (>95%) is observed, which is much better than that of nZVI within the same pH range (<40%) (Su et al., 2014a). The negatively charged surface of S-nZVI at this pH range likely contributes to increased Cd^{2+} removal. Below pH 8, Cd is present in solution entirely as Cd^{2+} (Boparai et al., 2013), so hydrolysis of Cd^{2+} or precipitation as $Cd(OH)_2$ at pH $\geq$ 8 (which is of importance for Cd removal by nZVI) is unlikely to significantly increase Cd removal by S-nZVI. Nevertheless, S-nZVI completely removes 40 mg/L Cd from water with pH $\geq$ 7 (Fig. 7). Overall, S-nZVI can efficiently immobilize Cd across a much wider range of pH than nZVI.
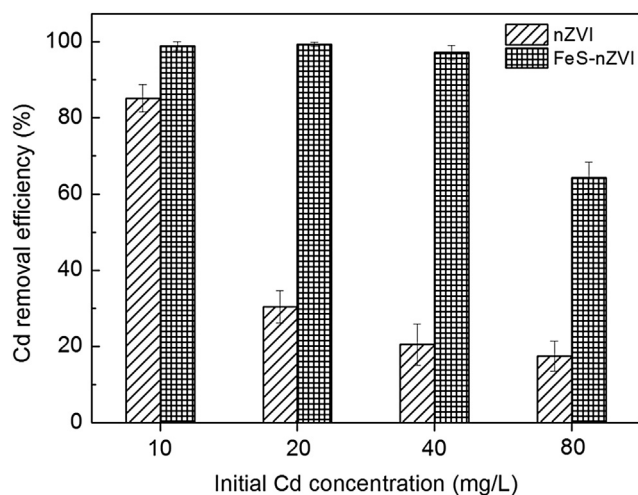
Fig. 8 – Cd removal efficiency of aged nZVI and FeS-nZVI (3 weeks old nanoparticle concentration = 500 mg/L).

### 3.5. Aging effect on Cd removal capacity of nZVI/S-nZVI

Previous studies concluded that aging had a negative influence on structure and pollutant removal performance of nZVI (Liu and Lowry, 2006) and FeS-nZVI (Kim et al., 2014). As seen from Eqs. (17) and (18), Fe^0 reacts with water (Liu and Lowry, 2006) and S^0 (within the particle core) (Chin et al., 2005) at low reaction rates, which is responsible for the decline of the reducing capacity and magnetic force of aged S-nZVI (Kim et al., 2014). TEM images (Fig. S12) show that both the core and flake-like structure of S-nZVI are impaired to some extent by aging.

The removal capacity of freshly-prepared nZVI and S-nZVI is 42.5 and 85 mg-Cd/g respectively (Fig. 3b); while that of 3-week old nZVI and S-nZVI is 30 and 98 mg-Cd/g respectively (Fig. 8). While aging has a clear negative effect on Cd removal by nZVI, it appears to enhance Cd removal by S-nZVI. Over time, aggregation (Adeleye et al., 2013; Reinsch et al., 2010) and shell transformation (Zhang et al., 2013) of nZVI could lead to the decrease in binding sites for Cd. Aggregation is not as rapid in S-nZVI because the FeS_x coating decreases magnetic attractions between the particles. Although the structure of S-nZVI is destroyed, the total amount of sulfhydryl (-SH) available to remove Cd may increase due to the breaking of the S—S dumbbell bond in iron polysulfide and the transformation of S^0 to S^{2-}. Increased −SH groups as S-nZVI aged lead to more binding sites, which also contribute to Cd removal.

$$Fe^0 + 2H_2O \rightarrow Fe^{2+} + H_2 + 2OH^- \tag{17}$$

$$S^0 + Fe^0 \rightarrow FeS \tag{18}$$

3.6. Removal performance of different metals by S-nZVI

Given the high affinity of S for metals (Table S1), S-nZVI is expected to have high removal capacity for other metals such as Ni, Co, Zn. With 500 mg/L nanoparticles, S-nZVI removes 98.8% of Ni, 73.8% of Co, 78.4% of Zn, and 84% of Cd when each initial metal concentration is 50 mg/L (Table 1). nZVI on the other hand removes much lower amount at the same initial concentrations: 59.4% of Ni, 59.6% of Co, 35.3% of Zn, and 30.2% of Cd (Table 1). S-nZVI has much higher surface to volume ratio (70.4 m^2/g, data not shown) due to the abundant flake-like structure, compared with nZVI (37.4 m^2/g, data not shown). This results in increased binding sites (mainly −SH) for metal ion adsorption (Eq. (19)).

$$\equiv Fe - SH + Me^{2+} + H_2O \rightarrow \equiv Fe - S - Me - OH + 2H^+ \ (Me = metal) \tag{19}$$
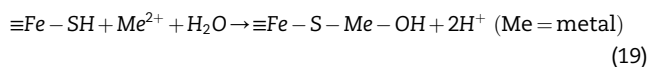
Table 1 – Removal efficiency of different heavy metals by nZVI and S-nZVI (Metal concentration = 50 mg/L; nanoparticle concentration = 500 mg/L).

Metal	Metal removal efficiency (%)	
	nZVI	S-nZVI
Ni	59.39 ± 5.63	98.81 ± 1.07
Co	59.63 ± 7.71	73.82 ± 4.24
Zn	35.32 ± 2.98	78.37 ± 3.31
Cd	30.20 ± 2.54	83.19 ± 2.85

Table 2 – Cd removal efficiency of nZVI and S-nZVI in different water matrices under nearly anoxic conditions (initial Cd concentration 50 mg/L, 500 mg/L particles).

Water body	Removal efficiency					
	2 h (%)		One month (%)		Two months (%)	
	nZVI	S-nZVI	nZVI	S-nZVI	nZVI	S-nZVI
Seawater	26.74 ± 6.13	97.85 ± 2.4	42.32 ± 4.13	98.20 ± 2.7	41.32 ± 2.13	99.90 ± 0.1
River-water	95.93 ± 3.64	93.74 ± 3.79	99.20 ± 0.28	99.99	99.23 ± 0.25	99.99
Groundwater	94.92 ± 3.19	88.29 ± 1.68	99.99	99.99	99.99	99.99
Wastewater	84.41 ± 4.43	64.84 ± 6.92	99.99	96.90 ± 3.11	99.99	97.40 ± 1.79
Nanopure-water	33.19 ± 8.23	78.98 ± 7.44	28.32 ± 6.58	61.20 ± 3.5	26.32 ± 8.84	60.70 ± 5.2

3.7. Cd removal performance of FeS-nZVI in different water matrices

To investigate the feasibility of practical application of S-nZVI in natural waters, batch tests of Cd removal in different water matrices were carried out. As seen in Table 2, S-nZVI can remove Cd efficiently from seawater (97.85%), river-water (93.74%), and groundwater (88.29%) after 2 h. Removal efficiency is 64.84% and 78.98% in wastewater and nanopure water after 2 h. A higher removal efficiency in seawater than in nanopure water (78.98%) suggests that high salinity does not reduce Cd sequestration by S-nZVI, unlike nZVI (Table 2). Speciation of Cd was modeled using Visual MINTEQ and we found that >99% of Cd exists as $CdCl_2$ in seawater due to the high concentration of chloride ions (Adeleye and Keller, 2014). $CdCl_2$ has low affinity for the surface of nZVI, which may have resulted in decreased Cd removal capacity in seawater by nZVI. High removal capacity of Cd by S-nZVI may be due to the high affinity between Cd^{2+} and S^{2-}.

Given that in real world remediation, the nanoparticles with sequestered Cd will settle to the sediment phase and mostly remain there, the stability of the Cd containing complex is very important. We measured the Cd concentration in supernatant after one and two months and results showed that except in nanopure water system, the sequestered Cd was not released back into the aqueous phase in the natural waters (Table 2). In addition, as seen in Fig. 7, release of Fe and S from S-nZVI is not expected to be significant at environmentally-relevant pH. This reduces the potential risk of using S-nZVI in the natural environment. Hence it may be practical to employ S-nZVI to treat Cd polluted water, regardless of water salinity and natural organic matter content.

4. Conclusions

In this study, S-nZVI was synthesized, characterized and employed in heavy metals removal experiments. TEM with EDS analysis suggested that sulfur was incorporated into the zerovalent iron core. SEM with EDS analysis indicated that S element was homogeneously distributed within the nanoparticles as well. S-nZVI had an optimal Cd removal capacity of 85 mg/g, which was >100% higher than pristine nZVI. Over 95% removal efficiency was achieved even at pH 5, indicating sulfide compounds played an important role in metals removal and chemical stability of particles. Oxygen impaired

the structure of S-nZVI but enhanced Cd removal capacity to about 120 mg/g. Aging did not have a negative effect on the removal capacity of S-nZVI, and Cd-containing mixtures remained stable in two months experiments. S-nZVI could efficiently immobilize dissolved metal ions from different contaminated water matrices.

Appendix A. Supplementary data

Supplementary data related to this article can be found at http://dx.doi.org/10.1016/j.watres.2015.02.004.

REFERENCES

Adeleye, A.S., Keller, A.A., 2014. Long-term colloidal stability and metal leaching of single wall carbon nanotubes: effect of temperature and extracellular polymeric substances. Water Res. 49, 236–250.

Adeleye, A.S., Keller, A.A., Miller, R.J., Lenihan, H.S., 2013. Persistence of commercial nanoscaled zero-valent iron (nZVI) and by-products. J. Nanoparticle Res. 15 (1), 1–18.

Bi, Y., Hayes, K.F., 2013. Nano-FeS inhibits UO_2 reoxidation under varied oxic conditions. Environ. Sci. Technol. 48 (1), 632–640.

Bi, Y., Hyun, S.P., Kukkadapu, R.K., Hayes, K.F., 2013. Oxidative dissolution of UO_2 in a simulated groundwater containing synthetic nanocrystalline mackinawite. Geochim. Cosmochim. Acta 102, 175–190.

Boparai, H.K., Joseph, M., O'Carroll, D.M., 2013. Cadmium (Cd(2+)) removal by nano zerovalent iron: surface analysis, effects of solution chemistry and surface complexation modeling. Environ. Sci. Pollut. Res. 20 (9), 6210–6221.

Cermak, V., Smutek, M., 1975. Mechanism of decomposition of dithionite in aqueous solutions. Collect. Czechoslov. Chem. Commun. 40 (11), 3241–3264.

Chen, P.J., Wu, W.L., Wu, K.C., 2013. The zerovalent iron nanoparticle causes higher developmental toxicity than its oxidation products in early life stages of medaka fish. Water Res. 47 (12), 3899–3909.

Chin, P.P., Ding, J., Yi, J.B., Liu, B.H., 2005. Synthesis of FeS$_2$ and FeS nanoparticles by high-energy mechanical milling and mechanochemical processing. J. Alloys Compd. 390 (1–2), 255–260.

Colvin, V., Goldstein, A., Alivisatos, A., 1992. Semiconductor nanocrystals covalently bound to metal surfaces with self-assembled monolayers. J. Am. Chem. Soc. 114 (13), 5221–5230.

Comba, S., Martin, M., Marchisio, D., Sethi, R., Barberis, E., 2012. Reduction of nitrate and ammonium adsorption using microscale iron particles and zeolitite. Water Air Soil Pollut. 223 (3), 1079–1089.

Crane, R.A., Scott, T.B., 2012. Nanoscale zero-valent iron: future prospects for an emerging water treatment technology. J. Hazard. Mater. 211–212, 112–125.

Dekkers, M.J., Schoonen, M.A.A., 1994. An electrokinetic study of synthetic greigite and pyrrhotite. Geochim. Cosmochim. Acta 58 (19), 4147–4153.

Gallegos, T.J., Fuller, C.C., Webb, S.M., Betterton, W., 2013. Uranium(VI) interactions with mackinawite in the presence and absence of bicarbonate and oxygen. Environ. Sci. Technol. 47 (13), 7357–7364.

Herbert Jr., R.B., Benner, S.G., Pratt, A.R., Blowes, D.W., 1998. Surface chemistry and morphology of poorly crystalline iron sulfides precipitated in media containing sulfate-reducing bacteria. Chem. Geol. 144 (1), 87–97.

Hota, G., Idage, S., Khilar, K.C., 2007. Characterization of nano-sized CdS–Ag$_2$S core-shell nanoparticles using XPS technique. Colloids Surfaces A Physicochem. Eng. Asp. 293 (1), 5–12.

Jayson, G.G., Parsons, B.J., Swallow, A.J., 1972. Oxidation of ferrous ions by hydroxyl radicals. J. Chem. Soc. Faraday Trans. 1: Phys. Chem. Condens. Phases 68, 2053–2058.

Jeong, H.Y., Klaue, B., Blum, J.D., Hayes, K.F., 2007. Sorption of mercuric ion by synthetic nanocrystalline mackinawite (FeS). Environ. Sci. Technol. 41 (22), 7699–7705.

Jeong, H.Y., Lee, J.H., Hayes, K.F., 2008. Characterization of synthetic nanocrystalline mackinawite: crystal structure, particle size, and specific surface area. Geochim. Cosmochim. Acta 72 (2), 493–505.

Kaushik, A., Jain, S., Dawra, J., Sharma, P., 2003. Heavy metal pollution in various canals originating from river Yamuna in Haryana. J. Environ. Biol. 24 (3), 331–337.

Keller, A.A., Garner, K., Miller, R., Lenihan, H., 2012. Toxicity of nano-Zero valent iron to freshwater and marine organisms. Plos One. http://dx.doi.org/10.1371/journal.pone.0043983.

Kim, J.Y., Park, H.J., Lee, C., Nelson, K.L., Sedlak, D.L., Yoon, J., 2010. Inactivation of Escherichia coli by nanoparticulate zerovalent iron and ferrous ion. Appl. Environ. Microbiol. 76 (22), 7668–7670.

Kim, E.J., Kim, J.H., Azad, A.M., Chang, Y.S., 2011. Facile synthesis and characterization of Fe/FeS nanoparticles for environmental applications. ACS Appl. Mater. Interfaces 3 (5), 1457–1462.

Kim, E.J., Murugesan, K., Kim, J.H., Tratnyek, P.G., Chang, Y.-S., 2013a. Remediation of trichloroethylene by FeS-Coated iron nanoparticles in simulated and real groundwater: effects of water chemistry. Ind. Eng. Chem. Res. 52 (27), 9343–9350.

Kim, E.J., Le Thanh, T., Kim, J.H., Chang, Y.S., 2013b. Synthesis of metal sulfide-coated iron nanoparticles with enhanced surface reactivity and biocompatibility. RSC Adv. 3 (16), 5338–5340.

Kim, E.J., Kim, J.H., Chang, Y.S., Turcio-Ortega, D., Tratnyek, P.G., 2014. Effects of metal ions on the reactivity and corrosion electrochemistry of Fe/FeS nanoparticles. Environ. Sci. Technol. 48 (7), 4002–4011.

Li, X.Q., Zhang, W.X., 2006. Iron nanoparticles: the core-shell structure and unique properties for Ni(II) sequestration. Langmuir 22 (10), 4638–4642.

Li, Y., Lu, A., Ding, H., Zeng, C., Yan, Y., Wang, X., Wang, C., 2012. Synergistic interaction between electricigens and natural pyrrhotite to produce active oxygen radicals. Geomicrobiol. J. 29 (3), 264–273.

Li, S.L., Wang, W., Yan, W.L., Zhang, W.X., 2014. Nanoscale zero-valent iron (nZVI) for the treatment of concentrated Cu(II) wastewater: a field demonstration. Environ. Sci. Process Impacts 16 (3), 524–533.

Liu, Y., Lowry, G.V., 2006. Effect of particle age (Fe^0 Content) and solution pH on NZVI reactivity: H$_2$ evolution and TCE dechlorination. Environ. Sci. Technol. 40 (19), 6085–6090.

Liu, J., Valsaraj, K.T., Devai, I., DeLaune, R.D., 2008. Immobilization of aqueous Hg(II) by mackinawite (FeS). J. Hazard. Mater. 157 (2–3), 432–440.

Mejia Likosova, E., Collins, R.N., Keller, J., Freguia, S., 2013. Anodic reactivity of ferrous sulfide precipitates changing over time due to particulate speciation. Environ. Sci. Technol. 47 (21), 12366–12373.

China, Ministry of Environmental Protection, Ministry of Land and Resources, 2014. Report of Soil Pollution in China. http://www.mep.gov.cn/gkml/hbb/qt/201404/W020140417558995804588.pdf.

Monteiro-Neto, C., Itavo, R.V., Moraes, L.E., 2003. Concentrations of heavy metals in Sotalia fluviatilis (Cetacea: Delphinidae) off the coast of Ceara, northeast Brazil. Environ. Pollut. 123 (2), 319–324.

Morgan, B., Rate, A.W., Burton, E.D., 2012. Trace element reactivity in FeS-rich estuarine sediments: influence of formation environment and acid sulfate soil drainage. Sci. Total Environ. 438, 463–476.

Murphy, R., Strongin, D.R., 2009. Surface reactivity of pyrite and related sulfides. Surf. Sci. Rep. 64 (1), 1–45.

Neal, A.L., Techkarnjanaruk, S., Dohnalkova, A., McCready, D., Peyton, B.M., Geesey, G.G., 2001. Iron sulfides and sulfur species produced at hematite surfaces in the presence of sulfate-reducing bacteria. Geochim. Cosmochim. Acta 65 (2), 223–235.

Reinsch, B.C., Forsberg, B., Penn, R.L., Kim, C.S., Lowry, G.V., 2010. Chemical transformations during aging of zerovalent iron nanoparticles in the presence of common groundwater dissolved constituents. Environ. Sci. Technol. 44 (9), 3455–3461.

Reinsch, B.C., Levard, C., Li, Z., Ma, R., Wise, A., Gregory, K.B., Brown, G.E., Lowry, G.V., 2012. Sulfidation of silver nanoparticles decreases Escherichia coli growth inhibition. Environ. Sci. Technol. 46 (13), 6992–7000.

Rickard, D., 1995. Kinetics of FeS precipitation: part 1. Competing reaction mechanisms. Geochim. Cosmochim. Acta 59 (21), 4367–4379.

Su, Y., Adeleye, A.S., Huang, Y., Sun, X., Dai, C., Zhou, X., Zhang, Y., Keller, A.A., 2014a. Simultaneous removal of cadmium and nitrate in aqueous Media by nanoscale zerovalent iron (nZVI) and Au doped nZVI particles. Water Res. 63, 102–111.

Su, Y., Adeleye, A.S., Zhou, X., Dai, C., Zhang, W., Keller, A.A., Zhang, Y., 2014b. Effects of nitrate on the treatment of Lead contaminated groundwater by nanoscale zerovalent iron. J. Hazard. Mater. 280, 504–513.

Tewari, P.H., Campbell, A.B., 1979. Dissolution of iron during the initial corrosion of carbon steel in aqueous H2S solutions. Can. J. Chem. 57 (2), 188–196.

Ulrich, S., 2004. SIDS Initial Assessment Report for SIAM 19: Germany. http://www.inchem.org/documents/sids/sids/7775146.pdf.

Yan, W., Lien, H.-L., Koel, B.E., Zhang, W.X., 2013. Iron nanoparticles for environmental clean-up: recent developments and future outlook. Environ. Sci. Process. Impacts 15 (1), 63–77.

Zhang, T., Yu, C., Zhao, N., 1993. The studies on removal of Cd(II) in wastewater with chitosan. Rare Metals Hard Alloy 6, 84–88 (in Chinese).

Zhang, Y., Su, Y., Zhou, X., Dai, C., Keller, A.A., 2013. A new insight on the core-shell structure of zerovalent iron nanoparticles and its application for Pb(II) sequestration. J. Hazard. Mater. 263 (2), 685–693.

Zhang, Y., Li, Y., Dai, C., Zhou, X., Zhang, W., 2014. Sequestration of Cd(II) with nanoscale zero-valent iron (nZVI): characterization and test in a two-stage system. Chem. Eng. J. 244, 218–226.